Pseudoscalar meson electromagnetic form factor at high Q^{2} from full lattice QCD

J. Koponen, A. C. Zimermmane-Santos, C. T. H. Davies, G. P. Lepage, and A. T. Lytle (HPQCD Collaboration)

The pseudoscalar meson electromagnetic form factor at high Q^2 from full lattice QCD

J. Koponen,[1, 2] A. C. Zimermmane-Santos,[1, 3] C. T. H. Davies,[1, *] G. P. Lepage,[4] and A. T. Lytle[1]

(HPQCD collaboration)[, †]

[1]SUPA, School of Physics and Astronomy, University of Glasgow, Glasgow, G12 8QQ, UK
[2]INFN, Sezione di Tor Vergata, Dipartimento di Fisica,
Università di Roma Tor Vergata, Via della Ricerca Scientifica 1, I-00133 Roma, Italy
[3]São Carlos Institute of Physics, University of São Paulo,
PO Box 369, 13560-970, São Carlos, SP, Brazil
[4]Laboratory for Elementary-Particle Physics, Cornell University, Ithaca, New York 14853, USA

We give an accurate determination of the vector (electromagnetic) form factor, $F(Q^2)$, for a light pseudoscalar meson up to squared momentum transfer Q^2 values of 6 GeV^2 for the first time from full lattice QCD, including u, d, s and c quarks in the sea at multiple values of the lattice spacing. Our results show good control of lattice discretisation and sea quark mass effects. We study a pseudoscalar meson made of valence s quarks but the qualitative picture obtained applies also to the π meson, relevant to upcoming experiments at Jefferson Lab. We find that $Q^2 F(Q^2)$ becomes flat in the region between Q^2 of 2 GeV^2 and 6 GeV^2, with a value well above that of the asymptotic perturbative QCD expectation, but well below that of the vector-meson dominance pole form appropriate to low Q^2 values. Our calculations show that we can reach higher Q^2 values in future to shed further light on where the perturbative QCD result emerges.

I. INTRODUCTION

Hitting one constituent of a bound state with a photon initiates a complicated process if the bound state is not to fall apart. The momentum gained must be redistributed between all the constituents so that the whole convoy can slew round into the new direction. A price is paid in terms of a reduced interaction strength between the photon and the bound state and this is known as the electromagnetic form factor - a function of the square of the (space-like) 4-momentum, q^2, transferred from initial to final state. When the bound state is a hadron, and held together by the strong interaction, the determination of the form factor becomes a case study for our understanding of Quantum Chromodynamics (QCD) as a function of q^2. Both experimental measurement [1] and theoretical calculation are important. As we show here, lattice QCD, now including a realistic QCD vacuum [2], can provide key theoretical results.

The π meson is one of the simplest hadrons, with a valence quark and antiquark chosen from u/d. At small values of squared momentum transfer, $Q^2 = -q^2$ up to 0.25 GeV^2, its electromagnetic form factor, $F_\pi(Q^2)$, has been measured directly by scattering from atomic electrons [3]. The form factor can be fitted to a simple pole form in this region and the pole mass (close to that of the vector, ρ [4]) can be related to the r.m.s. electric charge radius. Lattice QCD calculations of the π form factor at small values of Q^2 [5–12] give a theoretical determination that agrees well with experiment.

At the other extreme of the Q^2 range, very large values, a perturbative QCD treatment of the electromagnetic form factor becomes possible because the process in which the hard photon scatters from the quark or antiquark factorises from the distribution amplitudes which describe the quark-antiquark configuration in the meson [13, 14]. The hard scattering amplitude is inversely proportional to Q^2 and can be treated perturbatively in QCD because a high Q^2 photon must be accompanied by a high momentum gluon exchange between the meson constituents (see Figure 1). The asymptotic perturbative QCD prediction, as $Q^2 \to \infty$, is very simple because the distribution amplitude can be normalised using the pion decay constant ($f_\pi = 130.4$ MeV) [13, 15, 16]. This gives

$$F_\pi(Q^2) = \frac{8\pi\alpha_s f_\pi^2}{Q^2} \qquad (1)$$

but this is not expected to be valid until Q^2 values of tens of GeV^2 are reached [14]. Meanwhile, the approximately constant value of $Q^2 F_\pi(Q^2)$ from Eq. (1) is numerically very different from the results and trend seen at small Q^2. This means that there is a large gap to be filled in our understanding, extending to relatively high Q^2 values [17].

For Q^2 of a few GeV^2 an indirect experimental method must be used to determine F_π with scattering of electrons from the pion cloud around a proton [18–20]. The most recent results from Jefferson Lab [21–25] have reached $Q^2 = 2.45$ GeV^2 but extension to 6 GeV^2 is foreseen [1], starting in 2018, as a key experiment (E12-06-101) for the 12 GeV upgrade.

This is also a Q^2 region in which lattice QCD can be used to calculate the meson electromagnetic form factor directly, as we demonstrate here. The method is straightforward, and the same for all Q^2 values. To reach higher Q^2 values the participating meson 3-momentum and therefore energy must be increased. Both statistical errors and systematic errors from discretisation effects

————

*christine.davies@glasgow.ac.uk
†URL: http://www.physics.gla.ac.uk/HPQCD

will then increase, so it is important to have a high statistics calculation in a quark formalism with small discretisation errors. Previous lattice QCD calculations (see [26] for a review) that include u, d and s quarks in the sea [27–29] have concentrated on having many Q^2 values for different heavy pion masses at one value of the lattice spacing. This has enabled studies of pion mass dependence but precluded taking a continuum limit. See also [5] for a more extensive calculation but including only u and d quarks in the sea.

Here we are able to reach values of Q^2 of 6 GeV^2 with an accuracy of 10% by performing a high statistics calculation at a number of well-separated Q^2 values. Instead of studying π mesons we work consistently with a 'pseudopion', a pseudoscalar meson made of valence s quarks (denoted η_s), accurately tuned [30] on full QCD (with u, d, s and c quarks in the sea) ensembles of gluon field configurations at three values of the lattice spacing and two values of the sea u/d quark masses. We work with s quarks because it is numerically much faster to accumulate high statistics for a precise result, little dependence on the sea u/d mass is expected and finite-volume effects are negligible [31]. We use the Breit frame where the initial and final mesons have opposite spatial momenta, $\vec{p}_i = -\vec{p}_f$ and Q^2 is maximized for a given $\vec{p}$. By working at values of the lattice spacing that range over a factor of 1.7 we are able to show that discretisation errors are small for our formalism, even at relatively large Q^2, and to extrapolate to the zero lattice spacing continuum limit.

Our η_s mesons are qualitatively very similar to π mesons for the purposes of this study, because the s quark is light compared to QCD scales. Both the small-Q^2 pole form and very high Q^2 perturbative QCD results for the form factor can be readily determined and thus our lattice QCD results provide a clear comparison to these two pictures in the region of $0 < Q^2 < 6$ GeV^2. In future we can extend this work to even higher Q^2 and also calculate other form factors, inaccessible to experiment, which can be compared to perturbative QCD to understand the Q^2 range in which it becomes valid. Most importantly, our results show the way to accurate predictions for F_π from lattice QCD for the upcoming Jefferson Lab experiments [1].

II. LATTICE QCD CALCULATION

The electromagnetic, or vector, form factor for a pseudoscalar meson, P, is determined from

$$\langle P(p_f)|V_\mu|P(p_i)\rangle = F_P(p_i + p_f)_\mu, \qquad (2)$$

where V_μ is a vector current coupling to the photon. Here we use the temporal component of V and $\vec{p}_i = -\vec{p}_f$ so that the right-hand side of eq. (2) becomes $2EF_P$ with $Q^2 = |2\vec{p}_i|^2$.

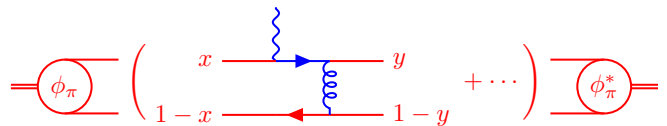The matrix element is determined in lattice QCD by combining information from meson '2-point' and '3-point'

FIG. 1: The perturbative QCD description of the π electromagnetic form factor. ϕ_π represents the distribution amplitude and the blue lines indicate the route of high momentum transfer through the hard scattering process.

functions [32]. 2-point functions tie together quark and antiquark propagators for a correlation function that creates a hadron at time 0 and destroys it at time t'. 3-point functions combine 3 propagators so that a meson is created at time 0, its quark (or antiquark) carrying momentum $\vec{p}_i$ interacts with a photon at time t and is scattered into $\vec{p}_f$, with the meson being destroyed at time T[1]. We fit the t'-, t- and T-dependence of the 2- and 3-point results (averaged over the gluon field configurations in an ensemble and including all results above a $t_{\min}$ of 3) simultaneously to a multi-exponential form in Euclidean time that includes the set of possible mesons made from this valence quark and antiquark [12]. This enables us to isolate the matrix element for the ground-state, lightest, meson and relate it to the required form factor, whilst making sure that systematic effects from the presence of higher mass states in the correlator are taken into account. We can normalise the form factor by the electric charge conservation requirement that $F_P(Q^2 = 0) = 1$.

We use the Highly Improved Staggered Quark (HISQ) formalism designed [34], and shown [31, 35–37], to have very small discretisation errors from the lattice spacing. We work on gluon field configurations generated by the MILC collaboration [38, 39] that include HISQ u, d, s and c quarks in the sea and also have a highly-improved gluon action [40]. On these configurations we study the η_s. In lattice QCD we can prevent this particle from mixing with other isospin zero mesons and then its properties can be well determined [31] and it behaves as a pseudopion; its mass is 688.5(2.2) MeV and decay constant 181.14(55) MeV. Here we determine its vector form factor as a function of Q^2.

Table I gives the parameters of the gluon field configurations we use, with lattice spacing varying from 0.15 fm to 0.09 fm and u/d quark mass either twice or five times the physical value, corresponding to $M_\pi \approx 216$ or 304 MeV. We tune the valence s quark mass on each ensemble to obtain the correct η_s mass [30]. We calculate η_s 2-point functions with a range of spatial momenta with magnitude in lattice units up to 0.62, given in Table I. These are implemented by using the 'twisted boundary condition' method [41] and are chosen to be in the (1,1,1) direction to minimise discretisation effects. We use η_s

---

[1] Charge-conjugation symmetry means that quark-line disconnected diagrams vanish in this case [33].

mesons made with the local γ_5 (Goldstone) operator; in staggered quark parlance this corresponds to spin-taste $\gamma_5 \otimes \gamma_5$ [34]. For our 3-point correlation functions we use a 1-link temporal vector current with spin-taste $\gamma_0 \otimes 1$.

We fit 2- and 3-point correlators simultaneously using Bayesian methods [42] to constrain fit parameters and determining the covariance between results at different Q^2 values. The fit forms are [31, 37]

$$
\begin{aligned}
C_{2pt}(\vec{p}) &= \sum_i b_i^2(p) \mathrm{f}(E_i(p), t') + \text{o.p.t.} \\
C_{3pt}(\vec{p}, -\vec{p}) &= \sum_{i,j} \big[b_i(p) \mathrm{f}(E_i(p), t) J_{ij}(Q^2) b_j(p) \times \\
&\qquad \mathrm{f}(E_j(p), T - t) \big] + \text{o.p.t.} \\
\mathrm{f}(E, t) &= e^{-Et} + e^{-E(L_t - t)}
\end{aligned}
\tag{3}
$$

The HISQ action gives opposite parity terms (o.p.t.) for η_s mesons at non-zero momentum; they are similar to the terms given explicitly above but with factors of $(-1)^{t'/a}$. The fit parameters are chosen to be the log of the ground-state energy, E_0, and the log of energy differences between the (ordered) excitations, i. For our kinematic set-up $F_{\eta_s}(Q^2) = J_{00}(Q^2)/J_{00}(0)$, with J_{00} the ground-state to ground-state amplitude. The division by $J_{00}(0)$ provides the normalisation of the lattice current. Results for the renormalisation factors inferred from $J_{00}(0)$ are given in Appendix A.

We use priors of 800 ± 400 MeV for the energy splitting between successive excitations and prior widths on amplitudes b_i and J_{ij} of at least 2 times the ground-state value. We take results from fits that include 6 exponentials where ground-state values and their uncertainties have stabilised and we have checked that the prior widths have only a minor impact on these uncertainties. Although we are only interested in ground-state properties here, our correlators are precise enough to resolve the first excited state. We have checked that its mass (around 950 MeV above the ground-state) is in reasonable agreement with that for an excited 0^- $s\bar{s}$ state seen in [43]. Note that we do not expect multi-meson (for example two kaon) energy levels to appear in our spectrum since the overlap of such states with our single meson operators is very small, being suppressed by the volume [44].

Results for the (ground-state) form factor are given in Table II and $Q^2 F(Q^2)$ is plotted in Figure 2. Results on different ensembles lie close to each other, showing that effects from discretisation and different u/d masses are very small. Tests of discretisation effects from studies of the meson energy and decay amplitudes as a function of spatial momentum are reported in Appendix B. We also show in Appendix B (see Figure 3) how statistical errors in the form factor grow as a function of Q^2 and $(Qa)^2$. It is in fact the statistical errors that provide a practical limit to how high in Q^2 we can reach here for different values of the lattice spacing. Note that the finer lattices have larger reach in Q^2 than the coarse.

To determine the form factor in the physical continuum limit we must extrapolate in the lattice spacing
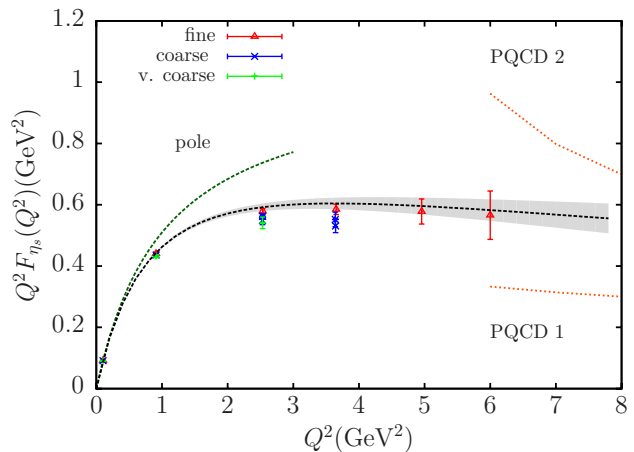

FIG. 2: Lattice QCD results for the vector form factor of the η_s meson, multiplied by Q^2 to focus on the large Q^2 behaviour, plotted as a function of Q^2. From coarse to fine: set 1 results are given by green pluses, set 2 by blue crosses, set 3 by blue bursts and set 4 by red triangles. Error bars include statistical/fit errors and uncertainties from the lattice spacing correlated between points. The black dashed line and grey band (for $\pm 1\sigma$) give the physical-point curve discussed in the text. The green dashed line marked 'pole' gives the pole form (P_ϕ^{-1}), for comparison. The orange dotted line marked 'PQCD 1' gives the asymptotic perturbative QCD prediction and that marked 'PQCD 2' includes non-asymptotic corrections to the distribution amplitude discussed in the text.

and sea u/d quark mass. We do this using a model-independent parameterisation of the form factor now standard in both theory and experiment for semileptonic weak decays (see [46] for a recent review), mapping the domain of analyticity in $t = q^2$ onto the unit circle in z. Since $z < 1$ we can then perform a power series expansion in z. We take [47]

$$
z(t, t_{\rm cut}) = \frac{\sqrt{t_{\rm cut} - t} - \sqrt{t_{\rm cut}}}{\sqrt{t_{\rm cut} - t} + \sqrt{t_{\rm cut}}}
\tag{4}
$$

where $t_{\rm cut}$ in our case is equal to $4M_K^2$. We choose the point that maps to $z = 0$ to be $q^2 = 0$, for simplicity; this gives $z_{\rm max}$ of 0.46 at $Q^2 = 6 \, {\rm GeV}^2$, well below 1. Rather than $F(Q^2)$ we work with $P_\phi(Q^2) F(Q^2)$, using $P_\phi(Q^2) = (1 + Q^2/M_\phi^2)$. The product $P_\phi F$ has reduced z-dependence because P_ϕ^{-1} is a good match to the form factor at small Q^2 (the ϕ being the $s\bar{s}$ vector meson) and it has the correct Q^{-2} dependence at large Q^2 (but the wrong value: see Figure 2). To combine a z-expansion with lattice QCD results we simply allow the coefficients in the expansion to have independent a- and $m_{\rm sea}$-dependence. Adapting the method from [48], we use the fit function

$$
P_\phi F(z, a, m_{\rm sea}) = 1 +
\tag{5}
$$

$$
\sum_{i=1}^{i_{\max}} z^i A_i \left[1 + B_i (a\Lambda)^2 + C_i (a\Lambda)^4 + D_i \frac{\delta m}{10} \right].
$$

TABLE I: We use MILC gluon field configurations [38, 39], with $\beta = 10/g^2$ the QCD coupling and L_s and L_t the lattice dimensions. w_0/a [31] gives the lattice spacing, a, in terms of the Wilson flow parameter, w_0 [45]; w_0=0.1715(9) fm from f_π [31]. Set 1 is 'very coarse', sets 2 and 3, 'coarse' and set 4, 'fine'. am_l, am_s and am_c are the sea quark masses ($m_l \equiv m_u = m_d$) in lattice units. am_s^{val} is the valence s mass and aM_{η_s} the corresponding η_s mass in lattice units. n_{cfg} gives the number of configurations; 16 random-wall time sources on each give high statistics. ap gives the magnitude of the meson spatial momentum for the form factor at non-zero Q^2. We further reduce uncertainties on set 2 at $pa = 0.6$ by averaging over 4 directions. We use 3 values of T/a for our 3pt-functions: 9, 12, 15 on set 1; 12, 15, 18 on sets 2 and 3 and 15,18 and 21 on set 4.

Set	β	w_0/a	am_l	am_s	am_c	am_s^{val}	aM_{η_s}	ap	$L_s/a \times L_t/a$	n_{cfg}
1	5.8	1.1119(10)	0.0130	0.0650	0.838	0.0705	0.54028(15)	0.1243,0.3730,0.6217	16×48	1020
2	6.0	1.3826(11)	0.0102	0.0509	0.635	0.0541	0.43135(9)	0.1,0.3,0.5,0.6($\times$ 4 dirns)	24×64	1053
3	6.0	1.4029(9)	0.00507	0.0507	0.628	0.0533	0.42636(6)	0.493,0.591	32×64	1000
4	6.3	1.9006(20)	0.0074	0.037	0.44	0.0376	0.31389(7)	0.0728,0.218,0.364,0.437,0.509,0.56	32×96	1008

TABLE II: Results for the vector form factor, with statistical error, at values of Q^2 given in GeV^2.

Set	Q^2	$F(Q^2)$	Q^2	$F(Q^2)$	Q^2	$F(Q^2)$	Q^2	$F(Q^2)$	Q^2	$F(Q^2)$	Q^2	$F(Q^2)$
1	0.1012	0.9003(9)	0.9109	0.4747(18)	2.531	0.2138(70)						
2	0.1012	0.9009(5)	0.9111	0.4786(10)	2.531	0.2170(51)	3.644	0.1456(59)				
3					2.533	0.2219(23)	3.640	0.1517(65)				
4	0.1014	0.9014(6)	0.9091	0.4843(9)	2.535	0.2286(22)	3.653	0.1602(42)	4.956	0.1167(82)	5.999	0.094(13)

Note that the lattice 'data' on the left-hand-side include correlations between results. The coefficients B_i and C_i account for dependence on the lattice spacing; we take $\Lambda = 1$ GeV $\approx \sqrt{t_{\text{cut}}}$ to allow for $(pa)^2$ and $(pa)^4$ terms in F. Independent coefficients at each order i allow for Q^2-dependent discretisation effects. Only even powers of a appear in the HISQ formalism and, because we work in the Breit frame with a fixed direction for $\vec{p}$, there is only one scale, p, that can appear coupled with a. Note that, by definition, there are no z-independent discretisation errors. In Figure 6 of Appendix B we show results for $Q^2 F_{\eta_s}(Q^2)$ at two values of Q^2 plotted against the square of the lattice spacing, showing more explicitly the size of discretisation effects. We also show there how well the fit function of eq. (5) is able to reproduce the discretisation effects, including their Q^2 dependence. D_i accounts for the heavier-than-physical quark masses in the sea, using $\delta m = \sum_{u,d,s}(m_q - m_q^{\text{tuned}})/m_s^{\text{tuned}}$ [30] and dividing by a factor of 10 to convert this to a suitable chiral perturbation theory expansion parameter. We take priors on the B_i, C_i and D_i of 0.0(1.0) but on B_1 of 0.0(5), because leading a^2 errors are suppressed by α_s in the HISQ formalism [34]. For the A_i, the coefficients of the z-expansion in the continuum and chiral limits, we take priors of 0.0(2.0), twice as conservative as the Bayesian probability function would suggest. We use $i_{\max} = 4$; adding higher terms has no impact and neither does adding $(a\Lambda)^6$ terms.

Our fit has a χ^2/dof of 0.3. The result at $a = 0$ and physical quark masses (i.e. $1 + \sum A_i z^i$) is plotted (converted back to Q^2 space) in Figure 2 and shows little deviation from the results on the fine lattices. The fitted parameters A_i and their covariance matrix are given in Appendix C.

III. DISCUSSION/CONCLUSIONS

Figure 2 shows the physical curve for $Q^2 F_{\eta_s}(Q^2)$ determined from our results for $0 < Q^2 < 7$ GeV^2. At small Q^2 it is compared to the pole form, $P_\phi^{-1}(Q^2)$. Our results show that the physical curve peels away from the pole form at $Q^2 \approx 1$ GeV^2 and then lies significantly below it. Also plotted in Figure 2, for $Q^2 > 6$ GeV^2, is the asymptotic perturbative QCD form (labelled PQCD 1) of Eq. (1), using f_{η_s} instead of f_π. For α_s we have used $\alpha_s(\overline{\text{MS}}, n_f = 3)$ at a scale of $Q/2$, since this is the momentum carried by the gluon when the quark and antiquark share the meson momentum equally. Our physical curve then lies significantly above this result at Q^2 of 6 GeV^2. We expect this qualitative picture of the physical curve to be true for the pion form factor to be determined in Jefferson Lab experiment E12-06-101 (the peeling away from the pole form is already apparent [25]).

For non-asymptotic Q^2 the leading perturbative QCD prediction is modified to [13, 14]:

$$F_P(Q^2) = \frac{8\pi f_P^2 \alpha_s(Q/2)}{Q^2} \left| 1 + \sum_{n=2}^{\infty} a_n^P(Q/2) \right|^2. \quad (6)$$

where the sum is over even n for a 'symmetric' meson (the η_s used here or π in the isospin limit). The a_n^P, coefficients of an expansion in Gegenbauer polynomials, evolve logarithmically to zero as $Q^2 \to \infty$.

Lattice QCD calculations have been used to determine a_2^π [49, 50] and this changes the asymptotic prediction substantially in the region of Q^2 around 10 GeV^2. The calculation of yet higher order corrections is complicated by operator mixing [51]. It is important to understand the limitations of the perturbative QCD approach here,

because the pion distribution amplitude inferred from $F_\pi(Q^2)$ is used in other calculations. They appear, for example, in light-cone sum rule calculations of the form factor at low q^2 for the exclusive weak decay $B \to \pi \ell \nu$ to determine V_{ub} [52, 53].

Figure 2 shows a curve (labelled PQCD 2) that uses a shape for the distribution amplitude $\phi_{\eta_s} = (x(1-x))^\zeta$ at a scale $Q/2 = 2\,\mathrm{GeV}$ where x is the light-cone momentum fraction and $\zeta = 0.52(6)$ is chosen to agree with lattice QCD results for a_2 for the π [50] (results indicate only weak quark mass-dependence, so this should be a good approximation). PQCD 2 is much higher than PQCD 1 at $Q^2 = 6\,\mathrm{GeV}^2$ and shows stronger Q^2-dependence. To obtain a flatter curve in better agreement with our results would require a broader distribution amplitude and a higher scale for α_s for less evolution. Such curves have been obtained for the π in a recent Dyson-Schwinger approach [54], and it would be interesting to see if it can reproduce our results for the η_s. For this purpose we give the parameters for our continuum curve in Appendix C.

To extend our results to higher values of Q^2 is possible on finer lattices where a given value of ap corresponds to a higher $|\vec{p}|$ in GeV. A Q^2 of 12 GeV^2 should be possible on 'superfine' lattices with $a = 0.06$ fm, and even 20 GeV^2 at $a = 0.045$ fm ('ultrafine'). Lower statistics calculations have already been done on such lattices [55–57]. See also [58] for new methods to reduce uncertainties in calculations at high Q^2. The scalar form factor at high Q^2 will give additional information since perturbative QCD [13, 14] predicts that this should fall more rapidly than Q^{-2}.

Perturbative QCD (Eq. 6) predicts approximate scaling of the form factor with the square of the decay constant, and we can test this in lattice QCD as we reduce the pseudoscalar meson mass towards that of the π. This scaling may set in before the Q^2-dependence becomes clearly that of perturbative QCD. If that is the case we can use our results here, rescaling by $(f_\pi/f_{\eta_s})^2$, to predict a value for $Q^2 F_\pi(Q^2)$ in a flat region from $2-6\,\mathrm{GeV}^2$ of $\approx 0.3\,\mathrm{GeV}^2$.

Appendix A: Renormalisation factors

Table III gives the values of the vector current renormalisation factor, Z_V, for each ensemble inferred from electric charge conservation at $Q^2 = 0$. The vector current we use is a 1-link current in the time direc-

TABLE III: Results for the renormalisation factor Z_V which multiplies the lattice temporal 1-link vector current used here to normalise the form factor fully nonperturbatively. The values are obtained from our fits at $Q^2 = 0$, using $Z_V = 1/J_{00}$.

Set	$Z_V^{s\bar{s}}$
1	1.3892(15)
2	1.3218(7)
3	1.3179(7)
4	1.2516(9)

tion, made gauge-invariant by the includion of an APE-smeared gauge link. The values for Z_V show the expected qualitative behaviour, slowly falling towards 1 on finer lattices.
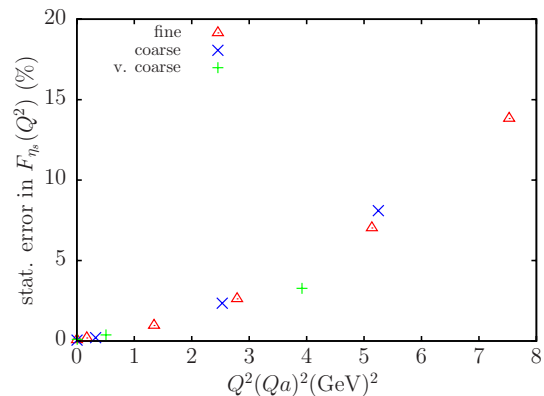

FIG. 3: The statistical uncertainty that we obtain in the form factor plotted as a function of $Q^2(Qa)^2$ for sets 1, 2 and 4 (green pluses, blue crosses and red triangles respectively). For set 2 at $pa = 0.6$ we have adjusted the error to be that for one spatial momentum direction (instead of 4) to match the statistics of the other points. Note that these results are specific to the Breit frame and teh values of T used here.

Appendix B: Tests of statistical errors and discretisation effects

In Figure 3 we show how the statistical error in the form factor result grows with Q^2. The results from different lattice spacing values (for approximately the same number of configurations, spatial lattice volume and smallest T value in physical units) appear to lie on a universal curve as a function of $Q^2(aQ)^2$. The curve is approximately quadratic, showing that uncertainties degrade rapidly at large pa values. However the same Q can be reached with smaller pa on finer lattices, moving down the curve. The plot helps to predict the statistical accuracy that will be obtained from calculations on other lattices using the same (Breit) frame.

A good test of discretisation errors is to study the ground-state meson energy as a function of spatial momentum and compare the speed of light (in units of c) obtained from $(E^2 - M^2)/\vec{p}^2$ to the expected value of 1.0
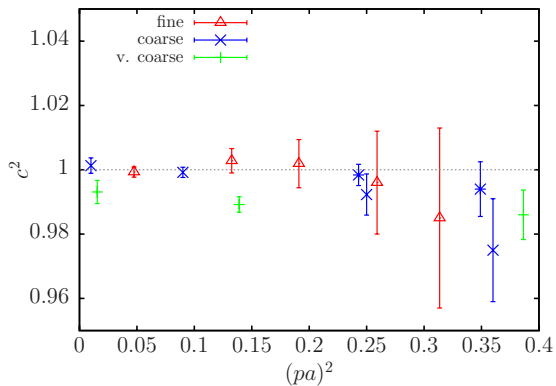
FIG. 4: The speed of light, defined in the text, determined from our η_s meson energies as a function of the square of their spatial momentum in lattice units. Note the expanded y-axis scale. Results from very coarse set 1 are given by green pluses, coarse set 2 by blue crosses and set 3 by blue bursts, and fine set 4 by red triangles.
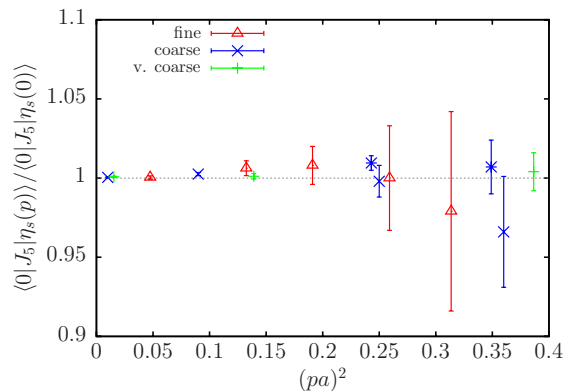

FIG. 6: We show here two slices through Figure 2 at two different values of Q^2, 2.53 GeV^2 and 0.91 GeV^2, plotted against the square of the lattice spacing. The points (symbols as for Fig. 4) show results at appropriate nearby values of Q^2 (see Table II) and include correlated uncertainties from the lattice spacing. The grey bands show our fit result using eq. (5), now as a function of a^2 but with δm set to zero.

FIG. 5: The ratio of the matrix element between vacuum and η_s of the pseudoscalar density at non-zero spatial momentum to that at zero momentum, as a function of the square of the meson spatial momentum in lattice units. Symbols as for Fig. 4.

in the absence of systematic discretisation effects. The ground-state energy, E, is given by $E_0(p)$ and the mass, M, by $E_0(0)$ from the 2-point fit function of eq. (3). Figure 4 shows results from our combined fits to the 2-point and 3-point η_s correlators used for our analysis. We see that, at the level of our statistical uncertainties (at most 3%), the speed of light shows no significant deviation from 1 even at the highest momenta that we use for our coarse and fine lattices. For very coarse set 1 there is a small (1%) but significant discrepancy at $pa = 0.373$. This is consistent with discretisation effects being dominated by $(ma)^4$ terms and therefore 3 times larger on the very coarse lattices than on the coarse. The statistical uncertainties increase with (pa) because the variance of the finite-momentum correlator overlaps with, and so is controlled by, the exponential behaviour of the square of the zero-momentum correlator. This behaviour is similar
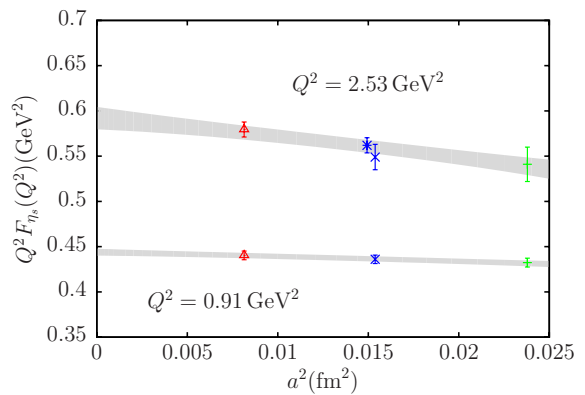
to that plotted in Figure 3 for the form factor. The uncertainties on the fine lattices at a given value of (pa) are larger than those on the coarse lattices, but the values of (pa) correspond to a larger value of $|\vec{p}|$, so the accuracy on the finer lattices translates into a larger reach in Q^2. Comparison of the two coarser lattices shows that the larger volume lattices have smaller statistical uncertainties at a given (pa) from volume-averaging.

A further test is to study the ratio of the matrix element of the pseudoscalar density, J_5, between the vacuum and the η_s meson at non-zero spatial momentum to that at zero momentum. Since the matrix element should be independent of momentum, we expect a result of 1.0. The matrix element is determined from the fitted amplitudes denoted by b_i in eq. (3), using

$$\frac{\langle 0|J_5|\eta_s(p)\rangle}{\langle 0|J_5|\eta_s(0)\rangle} = \frac{b_0(p)}{b_0(0)}\sqrt{\frac{E_0(p)}{E_0(0)}} \qquad \text{(B1)}$$

Figure 5 shows our results, with a very similar qualitative picture to that of Figure 4 and again showing excellent control of discretisation effects in the HISQ formalism.

Finally, in Figure 6, we illustrate the discretisation errors visible in the results for $Q^2 F_{\eta_s}(Q^2)$ plotted in Figure 2. The figure shows results at two different values of Q^2 for which we have calculations at three different values for the lattice spacing (see Table II), plotted against the square of the lattice spacing. The grey band shows the fit results from eq. (5) (for $\delta m = 0$) at these values of Q^2, as a function of a^2. We see that discretisation effects, although small, are clearly visible. Our fit form has no difficulty in fitting them and capturing their Q^2-dependence. The accuracy of our results at multiple (Qa) and a values is what allows us good control over the continuum limit for the range of Q^2 values that we cover here.

Appendix C: Parameters of the fit function

We give below the values of the fitted parameters, A_i and their covariance matrix obtained in the continuum and chiral limit of our results. In this limit we have (see eq. 5):

$$P_\phi F(z) = 1 + \sum_{i=1}^{4} A_i z^i \qquad (C1)$$

We find :

$$
\begin{aligned}
A_1 &= -0.387(59) \\
A_2 &= -0.87(26) \\
A_3 &= 0.4(1.0) \\
A_4 &= -0.5(1.7)
\end{aligned}
\qquad (C2)
$$

Only A_1 and A_2 are obtained with significance from the fit. The A_i have covariance matrix:

$$
\begin{bmatrix}
0.003472 & -0.008100 & 0.007133 & 0.000999 \\
-0.008100 & 0.068858 & -0.168850 & 0.151820 \\
0.007133 & -0.168850 & 1.021326 & -1.433623 \\
0.000999 & 0.151820 & -1.433623 & 2.81513
\end{bmatrix}
\qquad (C3)
$$

From the fit function for F we can readily derive results also for derivatives of F or $Q^2 F$. For example the mean square electric charge radius is given by

$$\langle r^2 \rangle_{\eta_s} = 6 \frac{dF}{dq^2}\bigg|_{q^2=0} \qquad (C4)$$

$$= \frac{6}{M_\phi^2}\left(1 - \frac{A_1}{4}\frac{M_\phi^2}{t_{\text{cut}}}\right) \qquad (C5)$$

Thus, from our results, we see that the mean square electric charge radius of the η_s is a factor of 1.103(16) larger than the naive expectation from the ϕ mass. Translating this into units of fm gives

$$\langle r^2 \rangle_{\eta_s} = 0.248(4)\,\text{fm}^2. \qquad (C6)$$

This is, not surprisingly, significantly smaller than the mean square electric charge radius of the π meson, for which the Particle Data Group give an average of $0.452(11)\,\text{fm}^2$ [59].

The slope of $Q^2 F$ is given from the fit parameters as:

$$
\begin{aligned}
\frac{d(Q^2 F_{\eta_s})}{dQ^2} &= F_{\eta_s} - \frac{Q^2 F_{\eta_s}}{P_\phi M_\phi^2} \\
&+ \frac{Q^2}{P_\phi}\frac{(1-z)\sum_i i A_i z^{i-1}}{2\sqrt{(t_{\text{cut}}+Q^2)}(\sqrt{t_{\text{cut}}+Q^2}+\sqrt{t_{\text{cut}}})}
\end{aligned}
\qquad (C7)
$$

Evaluating this at $Q^2 = 6\,\text{GeV}^2$ gives -0.014(8), consistent with zero (i.e. a curve for $Q^2 F$ that is flat at this point).

[1] G. M. Huber et al., Jefferson Lab Experiment E12-06-101 (http://www.jlab.org/exp_prog/proposals/06/PR12-06-101.pdf).

[2] C. Davies et al. (HPQCD, UKQCD, MILC and Fermilab Collaborations), Phys.Rev.Lett. **92**, 022001 (2004), hep-lat/0304004.

[3] S. Amendolia et al. (NA7 Collaboration), Nucl.Phys. **B277**, 168 (1986).

[4] W. R. Frazer and J. R. Fulco, Phys. Rev. Lett. **2**, 365 (1959).

[5] D. Brommel et al. (QCDSF/UKQCD), Eur. Phys. J. **C51**, 335 (2007), hep-lat/0608021.

[6] P. Boyle, J. Flynn, A. Jüttner, C. Kelly, H. P. de Lima, et al., JHEP **0807**, 112 (2008), 0804.3971.

[7] R. Frezzotti, V. Lubicz, and S. Simula (ETM Collaboration), Phys.Rev. **D79**, 074506 (2009), 0812.4042.

[8] S. Aoki et al. (JLQCD, TWQCD), Phys.Rev. **D80**, 034508 (2009), 0905.2465.

[9] O. H. Nguyen, K.-I. Ishikawa, A. Ukawa, and N. Ukita, JHEP **1104**, 122 (2011), 1102.3652.

[10] B. B. Brandt, A. Jüttner, and H. Wittig, JHEP **1311**, 034 (2013), 1306.2916.

[11] S. Aoki, G. Cossu, X. Feng, S. Hashimoto, T. Kaneko, J. Noaki, and T. Onogi (JLQCD), Phys. Rev. **D93**, 034504 (2016), 1510.06470.

[12] J. Koponen, F. Bursa, C. T. H. Davies, R. J. Dowdall, and G. P. Lepage, Phys. Rev. **D93**, 054503 (2016), 1511.07382.

[13] G. P. Lepage and S. J. Brodsky, Phys. Lett. **B87**, 359 (1979).

[14] G. P. Lepage and S. J. Brodsky, Phys. Rev. **D22**, 2157 (1980).

[15] G. R. Farrar and D. R. Jackson, Phys. Rev. Lett. **43**, 246 (1979).

[16] A. V. Efremov and A. V. Radyushkin, Phys. Lett. **94B**, 245 (1980).

[17] Department of Energy Nuclear Science Advisory Committee, Long Range Plan (2015) (http://science.energy.gov/np/nsac).

[18] P. Brauel, T. Canzler, D. Cords, R. Felst, G. Grindhammer, M. Helm, W. D. Kollmann, H. Krehbiel, and M. Schadlich, Phys. Lett. **B69**, 253 (1977).

[19] P. Brauel, T. Canzler, D. Cords, R. Felst, G. Grindhammer, M. Helm, W. D. Kollmann, H. Krehbiel, and

M. Schadlich, Z. Phys. **C3**, 101 (1979).

[20] H. Ackermann, T. Azemoon, W. Gabriel, H. D. Mertiens, H. D. Reich, G. Specht, F. Janata, and D. Schmidt, Nucl. Phys. **B137**, 294 (1978).

[21] J. Volmer et al. (Jefferson Lab F(pi)), Phys. Rev. Lett. **86**, 1713 (2001), nucl-ex/0010009.

[22] V. Tadevosyan et al. (Jefferson Lab F(pi)), Phys. Rev. **C75**, 055205 (2007), nucl-ex/0607007.

[23] T. Horn et al. (Jefferson Lab F(pi)-2), Phys. Rev. Lett. **97**, 192001 (2006), nucl-ex/0607005.

[24] H. P. Blok et al. (Jefferson Lab), Phys. Rev. **C78**, 045202 (2008), 0809.3161.

[25] G. M. Huber et al. (Jefferson Lab), Phys. Rev. **C78**, 045203 (2008), 0809.3052.

[26] B. B. Brandt, Int. J. Mod. Phys. **E22**, 1330030 (2013), 1310.6389.

[27] F. D. R. Bonnet, R. G. Edwards, G. T. Fleming, R. Lewis, and D. G. Richards (Lattice Hadron Physics), Phys. Rev. **D72**, 054506 (2005), hep-lat/0411028.

[28] H.-W. Lin and S. D. Cohen (2011), 1104.4319.

[29] A. J. Chambers et al. (UKQCD, QCDSF, CSSM) (2017), 1702.01513.

[30] B. Chakraborty, C. T. H. Davies, B. Galloway, P. Knecht, J. Koponen, G. C. Donald, R. J. Dowdall, G. P. Lepage, and C. McNeile, Phys. Rev. **D91**, 054508 (2015), 1408.4169.

[31] R. Dowdall, C. Davies, G. Lepage, and C. McNeile (HPQCD Collaboration), Phys.Rev. **D88**, 074504 (2013), 1303.1670.

[32] T. DeGrand and C. E. DeTar, *Lattice methods for quantum chromodynamics* (World Scientific, 2006).

[33] T. Draper, R. Woloshyn, W. Wilcox, and K.-F. Liu, Nucl.Phys. **B318**, 319 (1989).

[34] E. Follana, Q. Mason, C. Davies, K. Hornbostel, G. P. Lepage, et al. (HPQCD and UKQCD Collaborations), Phys.Rev. **D75**, 054502 (2007), hep-lat/0610092.

[35] E. Follana, C. Davies, G. Lepage, and J. Shigemitsu (HPQCD and UKQCD Collaborations), Phys.Rev.Lett. **100**, 062002 (2008), 0706.1726.

[36] C. Davies, C. McNeile, E. Follana, G. Lepage, H. Na, et al. (HPQCD Collaboration), Phys.Rev. **D82**, 114504 (2010), 1008.4018.

[37] G. Donald, C. Davies, R. Dowdall, E. Follana, K. Hornbostel, et al. (HPQCD Collaboration), Phys.Rev. **D86**, 094501 (2012), 1208.2855.

[38] A. Bazavov et al. (MILC collaboration), Phys.Rev. **D82**, 074501 (2010), 1004.0342.

[39] A. Bazavov et al. (MILC Collaboration), Phys.Rev. **D87**, 054505 (2013), 1212.4768.

[40] A. Hart, G. von Hippel, and R. Horgan (HPQCD Collaboration), Phys.Rev. **D79**, 074008 (2009), 0812.0503.

[41] D. Guadagnoli, F. Mescia, and S. Simula, Phys.Rev. **D73**, 114504 (2006), hep-lat/0512020.

[42] G. Lepage, B. Clark, C. Davies, K. Hornbostel, P. Mackenzie, et al., Nucl.Phys.Proc.Suppl. **106**, 12 (2002), hep-lat/0110175.

[43] J. J. Dudek, R. G. Edwards, B. Joo, M. J. Peardon, D. G. Richards, and C. E. Thomas, Phys. Rev. **D83**, 111502 (2011), 1102.4299.

[44] J. J. Dudek, R. G. Edwards, M. J. Peardon, D. G. Richards, and C. E. Thomas, Phys. Rev. **D82**, 034508 (2010), 1004.4930.

[45] S. Borsanyi, S. Durr, Z. Fodor, C. Hoelbling, S. D. Katz, et al., JHEP **1209**, 010 (2012), 1203.4469.

[46] R. J. Hill, eConf **C060409**, 027 (2006), hep-ph/0606023.

[47] G. Lee, J. R. Arrington, and R. J. Hill, Phys. Rev. **D92**, 013013 (2015), 1505.01489.

[48] J. Koponen, C. T. H. Davies, G. C. Donald, E. Follana, G. P. Lepage, H. Na, and J. Shigemitsu (2013), 1305.1462.

[49] R. Arthur, P. A. Boyle, D. Brommel, M. A. Donnellan, J. M. Flynn, A. Juttner, T. D. Rae, and C. T. C. Sachrajda, Phys. Rev. **D83**, 074505 (2011), 1011.5906.

[50] V. M. Braun, S. Collins, M. Gckeler, P. Prez-Rubio, A. Schfer, R. W. Schiel, and A. Sternbeck, Phys. Rev. **D92**, 014504 (2015), 1503.03656.

[51] V. Braun and D. Mueller, Eur. Phys. J. **C55**, 349 (2008), 0709.1348.

[52] A. Khodjamirian, T. Mannel, N. Offen, and Y. M. Wang, Phys. Rev. **D83**, 094031 (2011), 1103.2655.

[53] A. Bharucha, JHEP **05**, 092 (2012), 1203.1359.

[54] L. Chang, I. C. Cloet, C. D. Roberts, S. M. Schmidt, and P. C. Tandy, Phys. Rev. Lett. **111**, 141802 (2013), 1307.0026.

[55] C. McNeile, C. T. H. Davies, E. Follana, K. Hornbostel, and G. P. Lepage, Phys. Rev. **D82**, 034512 (2010), 1004.4285.

[56] C. McNeile, C. T. H. Davies, E. Follana, K. Hornbostel, and G. P. Lepage, Phys. Rev. **D85**, 031503 (2012), 1110.4510.

[57] C. McNeile, C. T. H. Davies, E. Follana, K. Hornbostel, and G. P. Lepage, Phys. Rev. **D86**, 074503 (2012), 1207.0994.

[58] G. S. Bali, B. Lang, B. U. Musch, and A. Schäfer, Phys. Rev. **D93**, 094515 (2016), 1602.05525.

[59] C. Patrignani et al. (Particle Data Group), Chin. Phys. **C40**, 100001 (2016).